

# Nature of Stripes in the Generalized $t - J$ Model Applied to The Cuprate Superconductors

Kai-Yu Yang<sup>1,2</sup>, Wei Qiang Chen<sup>2</sup>, T. M. Rice<sup>1,2</sup>, M. Sigrist<sup>1</sup>, Fu-Chun Zhang<sup>2</sup>

<sup>1</sup> *Institut für Theoretische Physik, ETH Zürich, CH-8093 Zürich, Switzerland*

<sup>2</sup> *Center for Theoretical and Computational Physics and Department of Physics,  
The University of Hong Kong, Hong Kong SAR, China*

(Dated: today)

## Abstract

Recent transport properties on the stripe phase in  $\text{La}_{1.875}\text{Ba}_{0.125}\text{CuO}_4$  by Li *et al.*<sup>1</sup> found 2-dimensional superconductivity over a wide temperature range including a Berezinski-Kosterlitz-Thouless transition at a temperature  $T=16\text{K}$ , with 3-dimensional superconducting (SC) ordering only at  $T=4\text{K}$ . These results contradict the long standing belief that the onset of superconductivity is suppressed by stripe ordering and suggest coexistence of stripe and SC phases. The lack of 3-D superconducting order above  $T=4\text{K}$  requires an antiphase ordering in the SC state to suppress the interlayer Josephson coupling as proposed by Berg *et al.*<sup>2</sup>. Here we use a renormalized mean field theory for a generalized  $t$ - $J$  model to examine in detail the energetics of the spin and charge stripe ordered SC states including possible antiphase domains in the SC order. We find that the energies of these modulated states are very close to each other and that the anisotropy present in the low temperature tetragonal crystal structure favors stripe resonating valence bond states. The stripe antiphase SC states are found to have energies very close, but always above, the ground state energy which suggests additional physical effects are responsible for their stability.

PACS numbers: 71.10.-w, 71.27.+a, 74.20.-z, 74.72.-h

## I. INTRODUCTION

Recently Li and coworkers<sup>1</sup> reported new results on transport properties of the stripe phase in  $\text{La}_{1.875}\text{Ba}_{0.125}\text{CuO}_4$ . They found that 2-dimensional superconducting (SC) fluctuations appear at an onset temperature  $T_c^{2D}$  (=42K) which greatly exceeds the critical temperature for 3-dimensional SC order,  $T_c$  (=4K). These results contradicted the long standing belief that the onset of SC behavior was suppressed to very low temperatures in the presence of the static spin and charge density wave (SDW and CDW hereafter) or more precisely spin and charge stripe orderings. Li *et al.*,<sup>1</sup> found strong evidence for a Berezinskii-Kosterlitz-Thouless transition (BKT) at  $T_{\text{BKT}}$  (=16K). This implies that the Josephson coupling between the  $\text{CuO}_2$  planes strictly vanishes for  $T > T_c$ . Shortly afterwards Berg *et al.*<sup>2</sup> proposed that the strict interplanar decoupling arises because the planar superconductivity contains a periodic array of lines of  $\pi$ -phase shift which rotate through  $\pi/2$  up the  $c$ -axis together with the spin and charge stripe ordering in the low temperature tetragonal (LTT) phase. SDW order also appears at the same onset temperature,  $T_c^{2D}$  in zero magnetic field and this temperature is clearly separated from the crystallographic transition temperature  $T_{co}$  separating the low temperature orthorhombic (LTO) and LTT phases. In this material the LTT phase shows a superlattice ordering at all temperatures below  $T_{co}$ .<sup>3</sup> Note however recent experiments by Fink *et al.* on  $\text{La}_{1.8-x}\text{Eu}_{0.2}\text{Sr}_x\text{CuO}_4$ <sup>4</sup> found different temperatures with the superlattice onset below the crystallographic phase transition temperature. Earlier studies by Lee *et al.* on superoxygenated  $\text{La}_2\text{CuO}_4$ <sup>5</sup> found the same onset temperature for both SC and SDW order ( $T=42\text{K}$ ). They also noted that signs of a CDW superlattice at higher temperature ( $T=55\text{K}$ ) has been reported. These temperatures coincide with the values found by Li *et al.* in  $\text{La}_{1.875}\text{Ba}_{0.125}\text{CuO}_4$  which suggests that Lee *et al.* were observing a similar stripe order with coexisting SDW and SC. In this case, however, the SC order is 3-dimensional, consistent with the absence of  $\pi/2$ -rotations in the crystal structure. These experiments lead us to conclude that in the presence of a CDW superlattice, coexisting SDW and antiphase d-wave SC can be favored.

Actually a similar ordering was suggested on general grounds earlier by Zhang<sup>6</sup> and also by Himeda, Kato and Ogata<sup>7</sup> on the basis of variational Monte Carlo calculations (VMC) for the strongly correlated one band  $t - t' - J$  model. Himeda *et al.*<sup>7</sup> found that a modulated state with combined SDW, and CDW and d-wave superconductivity (dSC)

containing site- or bond- centered anti-phase domain walls ( $\pi$ DW) ( a state we denote as SDW+CDW+APdSC<sup>s/b</sup>) had a lower energy than a uniform d-wave SC state over a wide range of parameters and was even lower than a modulated state without anti-phase (denoted as SDW+CDW+dSC<sup>s/b</sup>) in a narrower parameter range. Recent VMC and renormalized mean field theory (RMFT) calculations<sup>8</sup> have found that CDW+APdSC<sup>s/b</sup> state ( $\pi$ -DRVB state in ref.<sup>8</sup>) cost surprisingly little energy even in the absence of SDW modulations.

In this paper we report on calculations using the RMFT method to examine in greater detail the energetics of these novel modulated states within the generalized  $t - t' - t'' - J$  model. This method approximates the strong correlation condition of no double occupancy by Gutzwiller renormalization factors and generally agrees well with full VMC calculations which treat the strong correlation condition exactly. The static stripe phase appears in the LTT phase of La<sub>1.875</sub>Ba<sub>0.125</sub>CuO<sub>4</sub>. This crystallographic phase is entered at a temperature  $T_{co}$  ( $=52\text{K} > T_c^{2D}$ ) and displays a complex crystal structure which has not been fully determined to the best of our knowledge. Note that although the overall crystal structure is tetragonal the individual CuO<sub>2</sub> planes do not have square symmetry. Along one (x-) axis the Cu-O-Cu bonds are straight but in the perpendicular direction they are buckled<sup>9</sup>. Since the Cu-Cu distance is required to be the same in both directions there is a compressive stress along the x-axis which may well be the origin of the CDW superlattice that appears at the crystallographic phase transition into the LTT phase. At present the detailed displacements inside the supercell have not been refined. In our calculations we introduce a site dependent potential shift to mimic this effect. In addition we examine the effect of the hopping anisotropy between x- and y-axes which results from the different Cu-O-Cu bonding in the x and y directions. Such anisotropy was also considered by Capello *et al.*<sup>10</sup> in their work on stripes made from anti-phase shifts in the superconductivity.

## II. RENORMALIZED MEAN FIELD THEORY FOR THE EXTENDED $t - J$ MODEL

The  $t - J$  model was introduced in the early days of cuprate research by Anderson and by Zhang and Rice to describe lightly hole doped CuO<sub>2</sub> planes<sup>11</sup>. In this single band model configurations with doubly occupied sites are strictly forbidden due to the strong onsite Coulomb repulsion. The Hamiltonian takes the form, suppressing the constraint

$$\begin{aligned}
H_{tj} = & - \sum_{\langle i,j \rangle, \sigma} t_{(i,j)} \left( \hat{c}_{i,\sigma}^\dagger \hat{c}_{j,\sigma} + h.c. \right) + \sum_{\langle i,j \rangle} J_{(i,j)} \hat{\mathbf{S}}_i \cdot \hat{\mathbf{S}}_j \\
& + \sum_i V_i \hat{n}_i.
\end{aligned} \tag{1}$$

In the first term we include hopping processes between nearest neighboring (nn) sites (denoted by  $\langle i, j \rangle$ ), next neighboring sites (nnn) and 3rd neighboring sites (nnnn) on a square lattice with matrix elements  $t$ ,  $t'$ ,  $t''$  respectively. We will measure all energies in unit of  $t_0$  (300 meV) — a standard value for the nn hopping matrix element  $t$ . The superexchange spin-spin interaction between nn sites  $J = 0.3$ , and  $\sigma$  the spin index takes the value  $\pm$ . In addition we introduce a potential shift  $V_i$  which varies from site to site within the supercell to mimic the effect of the crystallographic superlattice in the LTT crystal structure. The strong coupling constraint of no double occupancy is very difficult to treat analytically. Zhang and coworkers introduced Gutzwiller renormalization factors to approximate the constraint<sup>12</sup>. This approximation has been shown to be quite accurate for mean field theories when compared to numerical evaluations by VMC of expectation values of the corresponding mean field wavefunctions,  $|\Psi\rangle$ , which are exactly projected down to the constrained Hilbert space<sup>13</sup>. Later the case of AF ordering was considered by Himeda and Ogata, who showed that an anisotropic spin renormalization term is required to reproduce the VMC results<sup>14</sup>. The resulting renormalized Hamiltonian is

$$\begin{aligned}
H = & - \sum_{\langle i,j \rangle, \sigma} g_{(i,j),\sigma}^t t_{(i,j)} \left( \hat{c}_{i,\sigma}^\dagger \hat{c}_{j,\sigma} + h.c. \right) \\
& + \sum_{\langle i,j \rangle} J_{(i,j)} \left[ g_{(i,j)}^{s,z} \hat{S}_i^z \hat{S}_j^z + g_{(i,j)}^{s,xy} \left( \hat{S}_i^+ \hat{S}_j^- + \hat{S}_i^- \hat{S}_j^+ \right) / 2 \right] \\
& + \sum_i V_i \hat{n}_i.
\end{aligned} \tag{2}$$

The renormalization factors  $g^t$ ,  $g^{s,xy}$  and  $g^{s,z}$  used to evaluate a projected mean field wavefunction depend on the local values of the magnetic and pairing order parameters and the local kinetic energy and hole density which are defined as follows

$$\begin{aligned}
m_i &= \langle \Psi_0 | \hat{S}_i^z | \Psi_0 \rangle; \\
\Delta_{\langle i,j \rangle, \sigma} &= \sigma \langle \Psi_0 | \hat{c}_{i,\sigma} \hat{c}_{j,-\sigma} | \Psi_0 \rangle; \\
\chi_{(i,j),\sigma} &= \langle \Psi_0 | \hat{c}_{i,\sigma}^\dagger \hat{c}_{j,\sigma} | \Psi_0 \rangle; \\
\delta_i &= 1 - \langle \Psi_0 | \hat{n}_i | \Psi_0 \rangle,
\end{aligned} \tag{3}$$

where  $|\Psi_0\rangle$  is the unprojected wavefunction. The two pairing amplitudes  $\Delta_{\langle i,j\rangle,\sigma=\pm}$  are treated independently to incorporate a possible triplet component. The explicit renormalization factors introduced first by Himeda and Ogata are quite complex,<sup>14</sup> and we use here a simpler form as follows,<sup>15</sup>

$$\begin{aligned}
g_{\langle i,j\rangle,\sigma}^t &= g_{i,\sigma}^t g_{j,\sigma}^t; \\
g_{i,\sigma}^t &= \sqrt{\frac{2\delta_i(1-\delta_i)}{1-\delta_i^2+4m_i^2} \frac{1+\delta_i+\sigma 2m_i}{1+\delta_i-\sigma 2m_i}}; \\
g_{\langle i,j\rangle}^{s,xy} &= g_i^{s,xy} g_j^{s,xy}; \\
g_i^{s,xy} &= \frac{2(1-\delta_i)}{1-\delta_i^2+4m_i^2}; \\
g_{\langle i,j\rangle}^z &= g_{\langle i,j\rangle}^{s,xy} \frac{2\left(\overline{\Delta}_{\langle i,j\rangle}^2 + \overline{\chi}_{\langle i,j\rangle}^2\right) - 4m_i m_j X_{\langle i,j\rangle}^2}{2\left(\overline{\Delta}_{\langle i,j\rangle}^2 + \overline{\chi}_{\langle i,j\rangle}^2\right) - 4m_i m_j}; \\
X_{\langle i,j\rangle} &= 1 + \frac{12(1-\delta_i)(1-\delta_j)\left(\overline{\Delta}_{\langle i,j\rangle}^2 + \overline{\chi}_{\langle i,j\rangle}^2\right)}{\sqrt{(1-\delta_i^2+4m_i^2)(1-\delta_j^2+4m_j^2)}},
\end{aligned} \tag{4}$$

where  $\overline{\Delta}_{\langle i,j\rangle} = \sum_{\sigma} \Delta_{\langle i,j\rangle,\sigma}/2$ ,  $\overline{\chi}_{\langle i,j\rangle} = \sum_{\sigma} \chi_{\langle i,j\rangle,\sigma}/2$ . Since the g-factors depends on the order parameters, the approach by direct diagonalization of the mean field Hartree-Fock Hamiltonian obtained from the Hamiltonian Eq[2] will not give the best energy of the Hamiltonian

$$\begin{aligned}
E_t &= \langle \Psi_0 | H | \Psi_0 \rangle \\
&= - \sum_{\langle i,j\rangle,\sigma} g_{\langle i,j\rangle,\sigma}^t t_{\langle i,j\rangle} [\chi_{\langle i,j\rangle,\sigma} + h.c.] \\
&\quad - \sum_{\langle i,j\rangle,\sigma} J_{\langle i,j\rangle} \left( \frac{g_{\langle i,j\rangle}^{s,z}}{4} + \frac{g_{\langle i,j\rangle}^{s,xy}}{2} \frac{\Delta_{\langle i,j\rangle,\overline{\sigma}}^*}{\Delta_{\langle i,j\rangle,\sigma}^*} \right) \Delta_{\langle i,j\rangle,\sigma}^* \Delta_{\langle i,j\rangle,\sigma} \\
&\quad - \sum_{\langle i,j\rangle,\sigma} J_{\langle i,j\rangle} \left( \frac{g_{\langle i,j\rangle}^{s,z}}{4} + \frac{g_{\langle i,j\rangle}^{s,xy}}{2} \frac{\chi_{\langle i,j\rangle,\overline{\sigma}}^*}{\chi_{\langle i,j\rangle,\sigma}^*} \right) \chi_{\langle i,j\rangle,\sigma}^* \chi_{\langle i,j\rangle,\sigma} \\
&\quad + \sum_i V_i n_i + \sum_{\langle i,j\rangle} g_{\langle i,j\rangle}^{s,z} J_{\langle i,j\rangle} m_i m_j
\end{aligned} \tag{5}$$

Instead, we minimize the energy with respect to the unprojected wave function  $|\Psi_0\rangle$  under the constraints  $\sum_i n_i = N_e$ ,  $\langle \Psi_0 | \Psi_0 \rangle = 1$ ,  $N_e$  is the total electron density. That is equivalent

to minimizing the function

$$W = \langle \Psi_0 | H | \Psi_0 \rangle - \lambda (\langle \Psi_0 | \Psi_0 \rangle - 1) - \mu \left( \sum_i \hat{n}_i - N_e \right) \quad (6)$$

which results in the following variational relation

$$\begin{aligned} 0 &= \frac{\delta W}{\delta \langle \Psi_0 |} \\ &= \sum_{\langle i,j \rangle, \sigma} \frac{\partial W}{\partial \chi_{\langle i,j \rangle, \sigma}} \frac{\delta \chi_{\langle i,j \rangle, \sigma}}{\delta \langle \Psi_0 |} + h.c. \\ &\quad + \sum_{\langle i,j \rangle, \sigma} \frac{\partial W}{\partial \Delta_{\langle i,j \rangle, \sigma}} \frac{\delta \Delta_{\langle i,j \rangle, \sigma}}{\delta \langle \Psi_0 |} + h.c. \\ &\quad + \sum_{i, \sigma} \frac{\partial W}{\partial n_{i, \sigma}} \frac{\delta n_{i, \sigma}}{\delta \langle \Psi_0 |} - \lambda | \Psi_0 \rangle. \end{aligned} \quad (7)$$

For an operator  $\hat{O}$  with the expectation value  $O = \langle \Psi_0 | \hat{O} | \Psi_0 \rangle$ ,  $\delta \langle \Psi_0 | \hat{O} | \Psi_0 \rangle / \delta \langle \Psi_0 | = \hat{O} | \Psi_0 \rangle$ . Thus one obtains the following mean field Hamiltonian,

$$\begin{aligned} H_{MF} &= \sum_{\langle i,j \rangle, \sigma} \frac{\partial W}{\partial \chi_{\langle i,j \rangle, \sigma}} \hat{c}_{i, \sigma}^\dagger \hat{c}_{j, \sigma} + h.c. \\ &\quad + \sum_{\langle i,j \rangle, \sigma} \frac{\partial W}{\partial \Delta_{\langle i,j \rangle, \sigma}} \sigma \hat{c}_{i, \sigma} \hat{c}_{j, \bar{\sigma}} + h.c. \\ &\quad + \sum_{i, \sigma} \frac{\partial W}{\partial n_{i, \sigma}} \hat{n}_{i, \sigma}, \end{aligned} \quad (8)$$

which satisfies the Schrödinger equation  $H_{MF} | \Psi_0 \rangle = \lambda | \Psi_0 \rangle$ . The coefficients of  $H_{MF}$  are given as

$$\begin{aligned} \frac{\partial W}{\partial \chi_{\langle i,j \rangle, \sigma}} &= -\delta_{\langle i,j \rangle, \langle i,j \rangle} J_{\langle i,j \rangle} \left( \frac{g_{\langle i,j \rangle}^{s,z}}{4} + \frac{g_{\langle i,j \rangle}^{s,xy}}{2} \frac{\chi_{\langle i,j \rangle, \bar{\sigma}}^*}{\chi_{\langle i,j \rangle, \sigma}^*} \right) \chi_{\langle i,j \rangle, \sigma}^* \\ &\quad - g_{\langle i,j \rangle, \sigma}^t t_{\langle i,j \rangle} + \left[ \frac{\partial W}{\partial \chi_{\langle i,j \rangle, \sigma}} \right]_g ; \\ \frac{\partial W}{\partial \Delta_{\langle i,j \rangle, \sigma}} &= -J_{\langle i,j \rangle} \left( \frac{g_{\langle i,j \rangle}^{s,z}}{4} + \frac{g_{\langle i,j \rangle}^{s,xy}}{2} \frac{\Delta_{\langle i,j \rangle, \bar{\sigma}}^*}{\Delta_{\langle i,j \rangle, \sigma}^*} \right) \Delta_{\langle i,j \rangle, \sigma}^* \\ &\quad + \left[ \frac{\partial W}{\partial \Delta_{\langle i,j \rangle, \sigma}} \right]_g ; \\ \frac{\partial W}{\partial n_{i, \sigma}} &= -(\mu - V_i) + \frac{1}{2} \sigma \sum_j g_{\langle i,j \rangle}^{s,z} J_{\langle i,j \rangle} m_j + \left[ \frac{\partial W}{\partial n_{i, \sigma}} \right]_g \end{aligned} \quad (9)$$

with  $\partial W/\partial\chi_{(i,j),\sigma}^* = [\partial W/\partial\chi_{(i,j),\sigma}]^*$ ,  $\partial W/\partial\Delta_{(i,j),\sigma}^* = [\partial W/\partial\Delta_{(i,j),\sigma}]^*$ ,  $\delta_{(i,j),\langle i,j \rangle} = 1$  only when  $i$  and  $j$  are nn, otherwise it equals 0, the partial derivative terms  $[\frac{\partial W}{\partial O}]_g$  in the above equations refer to the derivative of  $W$  with respect to the mean field  $O$  via the Gutzwiller  $g$ -factors (see Eq[4]). This mean field Hamiltonian  $H_{MF}$  in Eq[8] is then solved self-consistently. In the numerical calculations, we always diagonalize  $H_{MF}$  for a sample consisting of 257 supercells along the direction with periodic boundary condition unless stated explicitly otherwise.

### III. SIMPLIFIED MODEL: SITE-CENTERED ANTI-PHASE DOMAIN WALLS WITH D-WAVE SUPERCONDUCTIVITY

We begin the discussion of the results with the simplest case namely site-centered anti-phase domain walls in a d-wave superconductor (APdSC<sup>s</sup>). To this end we restrict the Hamiltonian to the two terms without SDW order, and solve it self-consistently without considering explicitly the doping dependence of  $g$ -factors,

$$H_s = - \sum_{\langle i,j \rangle, \sigma} (g^t t_0 + g^s J_0 \tilde{\chi}_{i,j}^*) \hat{c}_{i,\sigma}^\dagger \hat{c}_{j,\sigma} - \sum_{\langle i,j \rangle} g^s J_0 \tilde{\Delta}_{i,j}^* \hat{c}_{i,\uparrow}^\dagger \hat{c}_{j,\downarrow}^\dagger + h.c. \quad (10)$$

Note that  $\tilde{\chi}_{i,j} \neq \chi_{i,j}$ , and  $\tilde{\Delta}_{i,j} \neq \Delta_{i,j}$  but has the same symmetry as  $\Delta_{i,j}$ . To keep the model simple, we set  $\tilde{\chi}_{i,j} = \tilde{\chi}_p$  independent of  $\langle i,j \rangle$ , and  $g^t = 2\delta/(1+\delta)$ ,  $g^s = 4/(1+\delta)^2$  where  $\delta$  is the average doping away from half-filling. We consider first an isolated  $\pi$ DW which lies in the center ( $i_x = 28$ ) of a finite sample with open boundary condition along  $x$  direction and width  $L_x = 55$ . To this end we set  $|\tilde{\Delta}_{i,j}| = \tilde{\Delta}_p$  except for the bonds along the domain wall which are set to zero, i.e  $\tilde{\Delta}_{i,j}|_{i_x=j_x=28} = 0$ . The  $\pi$ -phase shift requires that for the two bonds  $\langle i,j \rangle$  and  $\langle i',j' \rangle$  which are located symmetrically on the two sides of the domain wall,  $\Delta_{i,j}|_{i_x,j_x \leq 28} = -\Delta_{i',j'}|_{i'_x,j'_x \geq 28}$ . The change of sign at the domain wall causes an Andreev bound state (ABS) to appear at the chemical potential which we take as the energy zero. This shows up clearly when we calculate the local density of states (LDOS) as illustrated in Fig[1a,b]. For the case of weak coupling in Fig[1a] a clear peak appears in the LDOS at zero energy for sites at or near the domain wall ( $i_x = 27, 28, 29$ ) while far away sites show peaks at the bulk gap edges and reduced values at zero energy. This behavior shows up also very clearly in the spatial dependence of the quasiparticle spectral

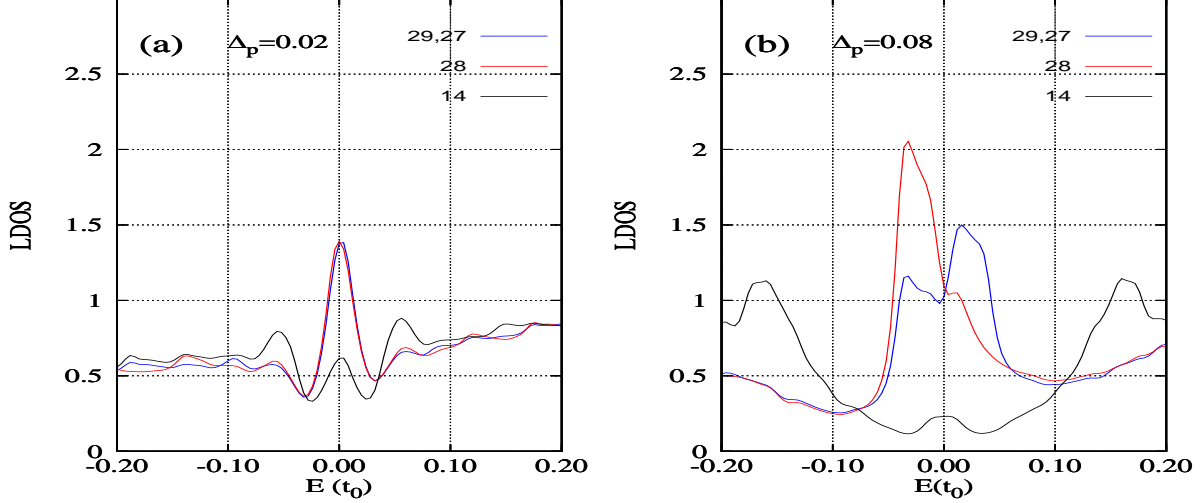


FIG. 1: (Color online) Local density of states (LDOS) for a simplified model (Hamiltonian  $H_s$  defined in Eq[10]) for an isolated site-centered anti-phase domain wall in a d-wave SC. Periodic boundary condition along y direction and open boundary condition along x direction are imposed. The width of the system along x direction is  $L_x = 55$  with the domain wall located at site 28. The average doping concentration is fixed at  $\delta = 0.25$ , and  $\tilde{\chi}_p = 0.20$ . Panels (a) and (b) are for  $\tilde{\Delta}_p = 0.02$ , and 0.08 respectively. The 14th site is halfway between the domain wall (site 28) and the edge, and the two sites (27, 29) are neighbors of the domain wall. A broadening factor  $0.004t_0$  is used.

weight. This is illustrated in Fig[2a,b] for the case of a weak and a moderate gap value of the pairing amplitude  $\tilde{\Delta}_p = 0.02(0.08)$ . The spectral weight is concentrated close to the  $\pi$ DW at quasiparticle energies  $E_k \simeq 0$ , but away from the  $\pi$ DW for values of  $E_k$  near the bulk gap energy  $E_k = 2g^s J_0 \tilde{\Delta}_p$ . The total energy differences between the states with and without  $\pi$ DW for the two  $\tilde{\Delta}_p$  are  $0.0066t_0$  and  $0.0365t_0$ , respectively. The energy cost of the domain wall is substantial, consistent with the creation of a LDOS peak in the center of energy gap. Note that for the case of a moderate gap value of  $\tilde{\Delta}_p$ , the peak of LDOS near  $E_k \simeq 0$  shows structures consistent with the development of a one-dimensional band of Andreev bound states which propagate along the domain wall. This can be also seen in the quasiparticle dispersion which is a function only of  $k_y$ .

Turning our attention to a periodic array of parallel  $\pi$ DW, we focus on the case of period  $L_x = 4$ , relevant to the cuprates, illustrated in Fig[3]. In this case the Andreev



bound states on neighboring domain walls will overlap strongly leading to a more complex dispersion relation for the associated quasiparticle states. Note the d-wave form of the bulk superconductivity leads to gapless excitations in the nodal directions which in turn leads to stronger overlap for near nodal quasiparticles. To illustrate this more complex behavior we focus on a particular model which can be solved analytically. To this end we set  $\delta = 0$  (i.e. half-filling),  $g^t = 0$  and set  $\tilde{\chi}_p = \tilde{\Delta}_p$  and  $g^s J \tilde{\chi}_p = 1$ . In this case the quasiparticle dispersion is obtained by diagonalizing the Hamiltonian

$$H_k = -\mathbf{X}_k^\dagger \begin{pmatrix} A_k & B_k \\ B_k^* & -A_{-k}^* \end{pmatrix} \mathbf{X}_k; \quad (11)$$

$$A_k = \begin{pmatrix} 2 \cos k_y & e^{ik_x} & 0 & e^{-ik_x} \\ e^{-ik_x} & 2 \cos k_y & e^{ik_x} & 0 \\ 0 & e^{-ik_x} & 2 \cos k_y & e^{ik_x} \\ e^{ik_x} & 0 & e^{-ik_x} & 2 \cos k_y \end{pmatrix};$$

$$B_k = \begin{pmatrix} 0 & e^{ik_x} & 0 & -e^{-ik_x} \\ e^{-ik_x} & -2 \cos k_y & e^{ik_x} & 0 \\ 0 & e^{-ik_x} & 0 & -e^{ik_x} \\ -e^{ik_x} & 0 & -e^{-ik_x} & 2 \cos k_y \end{pmatrix},$$

where  $\mathbf{X}_k^\dagger = (\hat{c}_{I,k,\uparrow}^\dagger, \hat{c}_{I,-k,\downarrow})$  with  $I = 1, 2, 3, 4$  denoting the sites inside a supercell. The quasiparticle dispersion takes a simple form,

$$E_k = \pm \sqrt{6 \cos^2 k_y + 4 \pm 2 \sqrt{(2 + \cos^2 k_y)^2 - 4 \sin^2 2k_x}}. \quad (12)$$

For a wavevector  $(k_x, k_y)$  close to  $(\pi/2, \pi/2)$ , the two quasiparticle bands close to the Fermi level have an anisotropic nodal structure with

$$E_k = \pm 2 \sqrt{K_x^2 + 2K_y^2}, \quad (13)$$

where  $(K_x, K_y) = (\pi/2 - k_x, \pi/2 - k_y)$ . This nodal structure completely suppresses the the density of states (DOS) at zero energy as shown in Fig[3], and pushes the peaks in the DOS of the Andreev bound states away from the chemical potential.

## IV. COEXISTING ANTI-PHASE SUPERCONDUCTIVITY AND SPIN AND CHARGE DENSITY WAVES

Anti-phase domain walls in a superconductor usually cost a substantial energy. The key question raised by the recent experimental results of Li *et al.*<sup>1</sup> on the static stripe phase is whether SDW and CDW coexisting with  $\pi$ DW lead to a state with a net energy gain. The VMC calculations of Himeda *et al.*<sup>7</sup> found a small energy gain for a longer superlattice with a larger separation between  $\pi$ DW within a restricted parameter range. Recent calculations for a 8-superlattice without SDW order by Raczkowski *et al.*<sup>8</sup> did not yield an energy gain but the energy cost to introduce  $\pi$ DW was quite small. These results motivated us to examine a wider parameter range within a RMFT approach and look for a possible net energy gain in an 8-superlattice (with site-centered anti-phase domain walls) at a hole concentration  $\delta = 1/8$  when coexisting SDW order and  $\pi$ DW are included. A longer 10-superlattice (with bond-centered anti-phase domain walls) state gives similar results. In view of the orthorhombic nature of the individual  $\text{CuO}_2$ -planes in the LTT phase, we allowed for anisotropy in the hopping  $t_{x(y)}$  and exchange coupling  $J_{x(y)}$ . Below we keep the nn hopping in the y-direction fixed,  $t_y = t_0$ , and scale  $J_x/J_y = t_x^2/t_y^2$ . In addition the presence of a crystallographic superlattice in the LTT phase motivated us to examine also the effect of the lattice inhomogeneity by including a site dependent potential modulation,  $V_i$ .

### A. Site-centered anti-phase dSC

The RMFT approximation yields a series of coupled nonlinear equations. An iteration method is used to obtain optimal values of the four order parameters: the pairing and hopping amplitudes, sublattice magnetization and hole density. When the solution iterates to a stable set of values we can conclude that a local energy minimum exists, but on occasion no stable solution can be found, which indicates that no local minimum exists with this symmetry. In general we find stable solutions for the case of coexisting CDW and SDW with or without  $\pi$ DW. Typical patterns for an 8-superlattice are illustrated in Fig[4] with or without site-centered  $\pi$ DW in systems where the modulation of the pairing amplitude is site centered. The antiferromagnetic domain wall (AFDW) coincides with the maximum hole

density while the  $\pi$ DW appears at the minimum hole density. (In the case without SDW, the  $\pi$ DW appears at the maximum hole density<sup>8</sup>.)

In table I the results for the ground state energy and local values of the order parameters are presented. The upper lines are for the case of nn hopping only ( $t' = 0$ ), with and without, anisotropic component in the nn hopping  $t_{x(y)}$ . In this case  $t_x = t_y$  the results show that the uniform AFM+dSC state is lowest. When AFDW and the associated modulation of the hole density are included the resulting state (denoted by SDW+CDW+dSC<sup>s</sup>) has an energy that is slightly higher. Introducing  $\pi$ DW to create antiphase superconducting order (SDW+CDW+APdSC<sup>s</sup>) raises the energy further. Anisotropy in the nn hopping narrows the energy differences but does not change the relative ordering of the states with and without  $\pi$ DW. When a weak nnn hopping is added, the SDW+CDW+dSC<sup>s</sup> state gains in energy and when anisotropy is also added this state has the lowest energy. In this case when we consider anisotropic nn hopping, the energy cost of introducing  $\pi$ DW in the superconducting is further reduced to small but still positive values. A further increase in the nnn hopping term (shown in Fig[5a]) however does not lead to an energy gain for  $\pi$ DW. The energy cost of  $\pi$ DW remains very small but positive.

The presence of substantial local modulations in the hole density in these states led us to investigate the effect of introducing a site dependent potential shift. Such a shift can result from the crystallographic superlattice modulation that appears at the crystallographic transition into the LTT state. The results in Fig[5b] show that this potential shift reduces the energy cost of the site-centered anti-phase domain wall and enhances the charge and spin modulation but still does not lead to a net energy gain for the SDW+CDW+APdSC<sup>s</sup> state even in the most favorable case of anisotropic nn hopping and substantial nnn hopping. Within the RMFT the  $\pi$ DW always demands an energy cost even though it may be only a very small amount. Bond-centered  $\pi$ DW with anisotropic nn hopping and longer periodicity  $L_x = 10$  shows that the energy difference between these two states, with and without  $\pi$ DW, can be also very close.

$t_x, t'$	state	$E_t$	$E_{kin}$	$E_J$	$\delta_{max}$	$\delta_{min}$	$m_{max}$	$\bar{\Delta}_{max}$	$\bar{\Delta}_{min}$	$\bar{\chi}_{max}$	$\bar{\chi}_{min}$
$t_x = 1.00$ $t' = 0.0$	AFM+dSC	-0.4878	-0.3287	-0.1593	0.12500	0.12500	0.08524	0.1142	0.1142	0.1903	0.1903
	dSC	-0.4863	-0.3428	-0.1435	0.12500	0.12500	0	0.1152	0.1152	0.1928	0.1928
	SDW+CDW+dSC <sup>s</sup>	-0.4865	-0.3373	-0.1492	0.1372	0.1134	0.08412	0.1214	0.09917	0.2215	0.1821
	SDW+CDW+APdSC <sup>s</sup>	-0.4782	-0.3292	-0.1490	0.1498	0.09604	0.1418	0.1114	0	0.2639	0.1111
$t_x = 0.85$ $t' = 0.0$	AFM+dSC	-0.4536	-0.3117	-0.1419	0.12500	0.12500	0.07432	0.08399	0.07724	0.2652	0.1098
	dSC	-0.4526	-0.3225	-0.1301	0.12500	0.12500	0	0.08409	0.07593	0.2675	0.1122
	SDW+CDW+dSC <sup>s</sup>	-0.4560	-0.3050	-0.1510	0.1737	0.07130	0.1720	0.06538	0.05154	0.2756	0.07822
	SDW+CDW+APdSC <sup>s</sup>	-0.4554	-0.3036	-0.1518	0.1815	0.05752	0.1871	0.04479	0	0.2866	0.06392
	SDW+CDW+dSC <sup>b</sup>	-0.4567	-0.3002	-0.1564	0.1911	0.06029	0.1831	0.06692	0.05151	0.2769	0.05869
	SDW+CDW+APdSC <sup>b</sup>	-0.4563	-0.2978	-0.1586	0.1988	0.04986	0.1941	0.06055	0	0.2841	0.03663
$t_x = 1.00$ $t_x = -0.1$	AFM+dSC	-0.4841	-0.3219	-0.1622	0.12500	0.12500	0.09356	0.1149	0.1149	0.1893	0.1893
	dSC	-0.4817	-0.3372	-0.1445	0.12500	0.12500	0	0.1179	0.1179	0.1920	0.1920
	SDW+CDW+dSC <sup>s</sup>	-0.4829	-0.3268	-0.1561	0.1525	0.1008	0.1268	0.1304	0.09917	0.2215	0.1654
	SDW+CDW+APdSC <sup>s</sup>	-0.4759	-0.3202	-0.1557	0.1650	0.08549	0.1731	0.09773	0	0.2642	0.1034
$t_x = 0.85$ $t' = -0.1$	AFM+dSC	-0.4507	-0.3056	-0.1451	0.12500	0.12500	0.08474	0.07982	0.07170	0.2688	0.1031
	dSC	-0.4490	-0.3182	-0.1308	0.12500	0.12500	0	0.08140	0.07155	0.2721	0.1054
	SDW+CDW+dSC <sup>s</sup>	-0.4539	-0.3024	-0.1515	0.1750	0.07336	0.1751	0.06401	0.04880	0.2742	0.08047
	SDW+CDW+APdSC <sup>s</sup>	-0.4533	-0.3021	-0.1512	0.1801	0.06318	0.1867	0.04286	0	0.1840	0.06953
	SDW+CDW+dSC <sup>b</sup>	-0.4538	-0.2991	-0.1547	0.1833	0.07206	0.1740	0.07046	0.05567	0.2728	0.07248
	SDW+CDW+APdSC <sup>b</sup>	-0.4533	-0.2972	-0.1560	0.1890	0.06202	0.1860	0.05946	0	0.2810	0.04685
$t_x = 1.00$ $t' = -0.3$	AFM+dSC	-0.4813	-0.3151	-0.1662	0.12500	0.12500	0.1188	0.1086	0.1086	0.1866	0.1866
	dSC	-0.4750	-0.3303	-0.1446	0.12500	0.12500	0	0.1216	0.1216	0.1899	0.1899
	SDW+CDW+dSC <sup>s</sup>	-0.4814	-0.3213	-0.1602	0.1709	0.09043	0.1746	0.1263	0.07922	0.2351	0.1280
	SDW+CDW+APdSC <sup>s</sup>	-0.4760	-0.3236	-0.1523	0.1700	0.09028	0.2002	0.07064	0	0.2431	0.1266
$t_x = 0.85$ $t' = -0.3$	AFM+dSC	-0.4491	-0.2986	-0.1506	0.12500	0.12500	0.1127	0.06892	0.05955	0.2683	0.09673
	dSC	-0.4436	-0.3122	-0.1314	0.12500	0.12500	0	0.08064	0.06819	0.2762	0.09695
	SDW+CDW+dSC <sup>s</sup>	-0.4523	-0.3008	-0.1515	0.1774	0.08221	0.1883	0.06455	0.04278	0.2681	0.08799
	SDW+CDW+APdSC <sup>s</sup>	-0.4518	-0.3017	-0.1501	0.1787	0.08034	0.1822	0.03503	0	0.2768	0.07811
	SDW+CDW+dSC <sup>b</sup>	-0.4513	-0.2985	-0.1528	0.1789	0.09117	0.1638	0.06976	0.04589	0.2680	0.08756
	SDW+CDW+APdSC <sup>b</sup>	-0.4506	-0.2984	-0.1523	0.1806	0.08737	0.1700	0.04898	0	0.2762	0.06648

TABLE I: Key results for various states obtained by selfconsistently solving the Hamiltonian in Eq[8] with an average hole density of 1/8. Listed are the mean field energy  $E_t$ , kinetic energy  $E_{kin}$ , spin-spin superexchange energy  $E_J$  and the modulation of hole concentration ( $\delta_{max}$  and  $\delta_{min}$ ), the largest antiferromagnetic moment ( $|m|_{max}$ ), pairing amplitude  $\bar{\Delta}_{max}$  and  $\bar{\Delta}_{min}$ , and  $\bar{\chi}_{max}$  and  $\bar{\chi}_{min}$  ( $\bar{\Delta} = \sum_{\sigma} \bar{\Delta}_{\sigma}$ ,  $\bar{\chi} = \sum_{\sigma} \chi_{\sigma}$ ) for various states including homogeneous AFM+dSC and dSC states, SDW+CDW+dSC<sup>s</sup> ( $L_x = 8$ ), SDW+CDW+APdSC<sup>s</sup> ( $L_x = 8$ ) and SDW+CDW+dSC<sup>b</sup> ( $L_x = 5$ ), SDW+CDW+APdSC<sup>b</sup> ( $L_x = 10$ ) states [APdSC (dSC) stands for d-wave SC state with (without) anti-phase domain walls site-centered (<sup>s</sup>) or bond-centered (<sup>b</sup>)]. The energy unit is  $t_0 = 300meV$ ,  $V \equiv 0$ ,  $J_x/J_y = t_x^2/t_y^2$ ,  $t_y = 1$ ,  $J_y = 0.3$ . Anisotropic nn hopping tends to energetically favor the homogeneous AFM+dSC state compared to the homogeneous dSC state. However, it also causes some inhomogeneous state to be energetically more favored, here for instance, the SDW+CDW+dSC<sup>s</sup> state. Note that to introduce anti-phase domain wall in the pairing order parameter in the renormalized mean field theory for the  $t - J$  model always cost energy, although it can be very small.

## B. Bond-centered anti-phase dSC

Alternative bond-centered anti-phase modulations of the pairing amplitude were considered by several groups.<sup>7,8,10</sup> In the case of the 8-superlattice we did not find any stable bond centered solution with nonzero SDW in the doping regime around 1/8 when requiring there is antiferromagnetic domain wall ( $m_I = 0$ ). But for longer periodicity  $L_x=10$  we found a stable solution. In Fig[6] a typical pattern for this long 10-superlattice with and without the bond-centered  $\pi$ DW is illustrated. The energy cost of the APdSC<sup>b</sup> is also positive for the bond-centered case but is even smaller compared with the site-centered case (see table I) at some cases.

## V. SPECTRAL PROPERTIES OF THE MODULATED PHASES

Next we examine the density of states in the modulated phases which gives us insight into the interplay between the SDW and SC with either dSC or APdSC order in the stripe phases. We restrict our considerations to the case of site-centered pairing modulation relevant for 8-superlattice. It is instructive to calculate several density of states, starting with the local density of states (LDOS)

$$A_I(\omega) = -\frac{1}{\pi} \sum_{\sigma} \text{Im} G_{I,\sigma}(\omega), \quad (14)$$

where  $G_{I,\sigma}(\omega)$  is the Fourier transform of the time dependent onsite Green's function  $G_{I,\sigma}(t) = -i \langle T_t c_{I,\sigma}(t) c_{I,\sigma}^{\dagger}(0) \rangle$ . The averaging of the LDOS over all sites gives

$$\bar{A}(\omega) = 1/N_c \sum_I A_I(\omega), \quad (15)$$

where  $N_c$  is the size of a supercell. Also of interest is the quasiparticle (QP) density of states

$$N(\omega) = \frac{1}{V_{RBZ}} \int dk \sum_l \delta(\omega - E_k^l), \quad (16)$$

where  $l$  denotes all the quasiparticle bands in the reduced Brillouin zone (RBZ),  $V_{RBZ}$  is the volume of RBZ,  $k \in \text{RBZ}$ . This latter is the density of states which determines the sum of the quasiparticle eigenvalues which enters the ground state energy in mean field theory. The results for these DOS in the various modulated phases are presented below. First we consider the cases of a dSC with array of  $\pi$ DW and of a SDW separately and then the results when both orders coexist.

### (a) anti-phase dSC

We start with the DOS for an array of  $\pi$ DW with a superlattice periodicity of 8 and an average hole density of  $1/8$ . The LDOS is shown in Fig[7], for the 3 independent lattice sites, site 1 at the  $\pi$ DW, site 3 halfway between the  $\pi$ DW and the remaining equivalent sites 2, 4. In the energy region near zero, the prominent features are a finite LDOS at all sites, which is largest at the center of a  $\pi$ DW (site 1) and two sharp peaks (labeled as A and B) symmetrically placed at positive and negative energies. The finite LDOS at  $E = 0$  implies a finite quasiparticle Fermi surface in this APdSC<sup>s</sup> state. The quasiparticle energy dispersion is quite complex and is illustrated in Fig[7c]. Along the high symmetry line,  $k_x = 0$ , in RBZ there are 3 nodal points. These expand into nodal lines for finite  $k_x$  to create two closed Fermi loops shown in Fig[7a]. The two sharp peaks labeled A and B in the DOS,  $\bar{A}(\omega)$ , can be shown to originate from the almost flat bands displaced away from zero energy in Fig[7c]. The LDOS that appears in Fig[7d] shows clearly an enhanced DOS near zero energy which implies a substantial energy cost to introduce the  $\pi$ DW into a uniform dSC state.

### (b) SDW

The second case we considered is a simple SDW state in which an array of AFDW is introduced to create a 8-superlattice. Again the LDOS (see Fig[8]) shows finite values at zero energy with the largest value at the center of the AFDW ( $m_i = 0$ ). As a consequence this SDW state is metallic. Note a uniform state would also be metallic at this hole concentration of  $\delta = 1/8$ . It is however very relevant that the SDW superlattice does not truncate the Fermi surface completely to give an insulating state, since then coexistence with d-wave pairing would be disfavored. Further any coexisting state would not be superconducting. The Fermi surface shown in Fig[8a] consists of standing waves along  $k_y$  *i.e.* perpendicular to the AFDW and two one-dimensional bands propagating along AFDW.

### (c) Coexisting SDW, CDW and dSC or anti-phase dSC

We examine the coexisting state to look for possible synergy between the SDW and dSC and also to compare the two possibilities for the superconducting uniform dSC and the APdSC<sup>s</sup>, *i.e.* superconductivity without and with an array of  $\pi$ DW. The favorable choice of the relative position of the two domain walls is to stagger the  $\pi$ DW and AFDW as shown in Fig[4]. From Fig[9a,b] one sees that in both cases the LDOS develops a strong minimum around zero energy with even a drop to zero in a narrow range around zero energy. The site dependence of the LDOS is weaker than in the previous cases. This strong energy minimum

indicates a certain synergy between the SDW and dSC which can lower the energy through a truncation of the finite Fermi surface that exists in the both cases separately, SDW and APdSC<sup>s</sup>. The energy difference in the LDOS between the two cases with and without  $\pi$ DW, is small. But when one compares the total ground state energy, a finite energy cost to introduce  $\pi$ DW into the superconductivity always appears.

The strong minimum in the DOS at the Fermi level in the SDW+CDW+APdSC<sup>s</sup> state is consistent with the spectra obtained in angle resolved photoemission (ARPES) and scanning tunnelling (STM) experiments on  $\text{La}_{1.875}\text{Ba}_{0.125}\text{CuO}_4$  reported by Valla *et al*<sup>16</sup>. Our calculations give a complex quasiparticle dispersion associated with the 8-fold superlattice which does not seem to be resolved in the ARPES spectra. So a more detailed comparison with experiment is not possible at this time but the main feature of the experimental DOS is reproduced in our calculations.

## VI. DISCUSSION

Anti-phase domain wall or  $\pi$ DW generally cost considerable energy in a superconductor because they generate an Andreev bound state at the Fermi energy due to the interference between reflected electrons and holes. This effect is illustrated in Fig[1a] which shows a peak in the LDOS centered on an isolated  $\pi$ DW. In an array of parallel  $\pi$ DW this DOS peak broadens into a 2-dimensional band due to both the propagation of the ABS along the  $\pi$ DW, as illustrated in Fig[1b], and the overlap of the ABS on neighboring  $\pi$ DW. This leads to structure which can lead to a pronounced minimum in the LDOS in certain cases such as the case of a closely spaced array of  $\pi$ DW shown in Fig[3b]. This structure in the LDOS lowers the energy cost to introduce  $\pi$ DW in the dSC, but leaves it still positive. For the period 8 supercell the modification of the DOS is less important. As illustrated in Fig[7c] the APdSC<sup>s</sup> bandstructure is quite complex and displays a finite Fermi surface (see Fig[7a]). The resulting LDOS has a finite value at the Fermi energy which is largest at the center of the  $\pi$ DW.

In the case of coexisting SDW and CDW one must first consider how the effect of these superlattices alone. The results are presented in Fig[8] which shows a metallic state with a finite DOS and Fermi surface. This is important since if the SDW resulted in an insulating groundstate, the addition of Cooper pairing would be less energetically favorable and would

not change the state from insulating to superconducting. The bandstructure consists of standing waves in the direction perpendicular to the AFDW which are propagating in the direction parallel to the AFDW.

Coexisting SDW and dSC leads to a substantial interplay between the two broken symmetries. Recently Agterberg and Tsunetsugu showed that there can be a synergy between the two orders due to the presence of cross terms involving both order parameters in a Landau expansion<sup>17</sup>. The cross term depends crucially on the relative orientation of the wavevector of the SDW and APdSC. For the case of parallel  $\mathbf{q}$ -vectors under consideration here (eg. as illustrated in Fig[6]), however the cross term vanishes. Nonetheless in the present case there is still a considerable synergy between the two broken symmetries. This shows up in the DOS as a pronounced dip at the chemical potential as illustrated in Fig[9b]. However, this effect is not confined to case of APdSC but is also present in the case of a uniform phase dSC coexisting with SDW as illustrated in Fig[9a]. We have not found a simple explanation for this synergy. The quasiparticle bands in the vicinity of the Fermi energy have a complex dispersion for which we do not have a simple interpretation. Remarkably the form of the DOS near the Fermi energy is very similar for coexisting SDW and dSC with and without the array of  $\pi$ DW the dSC. This subtle difference in the DOS shows up as only a small difference in the ground state energy so that the energy cost of introducing  $\pi$ DW is very small.

## VII. CONCLUSIONS

The small energy difference that we find agrees with the earlier calculations reported by Himeda *et al.*<sup>7</sup> for coexisting SDW and APdSC<sup>s/b</sup>. These authors used a VMC method in which the strong coupling onsite constraint is exactly treated whereas here it is only approximated through the Gutzwiller factors. This suggests that our failure to find a clear explanation for the stabilization of APdSC<sup>s/b</sup> does not result from the Gutzwiller approximation but may be because the t-J model omits some relevant physical effect. Alternatively the special cross term between SDW and APdSC order found by Agterberg and Tsunetsugu<sup>17</sup> which favors oblique wavevectors for the two periodicities may mean that our simple pattern with parallel arrays of AFDW and  $\pi$ DW is not optimal, although on the surface it looks very plausible to simply stagger the two domain walls. After completing this paper, we learned



that a related work was posted by Chou *et al.*<sup>18</sup>.

## VIII. ACKNOWLEDGES

We are grateful to John Tranquada, Alexei Tsvelik and Daniel Agterberg for stimulating discussions. KYY, TMR and MS gratefully acknowledge financial support from the Swiss Nationalfonds through the MANEP network. This work was also in part supported by RGC at HKSAR (FCZ and WQC).

- 
- <sup>1</sup> Q. Li, M. Huecker, G. D. Gu, A. M. Tsvelik, J. M. Tranquada, Phys. Rev. Lett. **99**, 067001 (2007).
  - <sup>2</sup> E. Berg, E. Fradkin, E.-A. Kim, S. A. Kivelson, V. Oganesyan, J. M. Tranquada, and S. C. Zhang, Phys. Rev. Lett. **99**, 127003 (2007).
  - <sup>3</sup> Young-June Kim, G. D. Gu, T. Gog, and D. Casa, Phys. Rev. B **77**, 064520 (2008).
  - <sup>4</sup> J. Fink, E. Schierle, E. Weschke, J. Geck, D. Hawthorn, H. Wadati, H.-H. Hu, H. A. Durr, N. Wizen, B. Buchner, G.A. Sawatzky, arXiv:0805.4352 (2008).
  - <sup>5</sup> Y.S. Lee, R.J. Birgeneau, M.A. Kastner, Y. Endoh, S. Wakimoto, K. Yamada, R.W. Erwin, S.H. Lee, G. Shirane, Phys. Rev. B **60** 3643 (1999).
  - <sup>6</sup> S.-C. Zhang, J. Phys. Chem. Solids **59**, 1774 (1998).
  - <sup>7</sup> A. Himeda, T. Kato, and M. Ogata, Phys. Rev. Lett. **88**, 117001 (2002).
  - <sup>8</sup> M. Raczowski, M. Capello, D. Poiblanc, R. Fresard, A. M. Oles, Phys. Rev. B **76**, 140505(R) (2007).
  - <sup>9</sup> B. Buchner, M. Breuer, A. Freimuth and A. P. Kampf, Phys. Rev. Lett. **73**, 1841 (1994).
  - <sup>10</sup> M. Capello, M. Raczowski, D. Poiblanc, Phys. Rev. B **77** 224502 (2008).
  - <sup>11</sup> P. W. Anderson, Science **235** 1196 (1987); F. C. Zhang and T. M. Rice Phys. Rev. B **37**, 3759 (1988).
  - <sup>12</sup> F. C. Zhang, C. Gros, T. M. Rice, H. Shiba, Supercon. Sci. Technol. **1**, 36(1988) or cond-mat/0311604 (2003).
  - <sup>13</sup> P. W. Anderson, P. A. Lee, M. Randeria, T. M. Rice, N. Trivedi, and F. C. Zhang, J. Phys. Condens. Matter **16**, R755 (2004); K. Y. Yang, C.T. Shih, C. P. Chou, S. M. Huang, T. K. Lee,

- T. Xiang, and F. C. Zhang, Phys. Rev. B **73**, 224513 (2006).
- <sup>14</sup> A. Himeda, and M. Ogata, Phys. Rev. B **60**, R9935 (1999); M. Ogata, and A. Himeda, Journal of the Physical Society of Japan, **72**, 374-391 (2003).
- <sup>15</sup> In the original form introduced by Himeda and Ogata<sup>14</sup>,  $g_{\langle i,j \rangle}^{s,xy} = g_i^{s,xy} g_j^{s,xy} a_{\langle i,j \rangle}^{-7}$ . The factor  $a_{\langle i,j \rangle}$  is very complicated but takes a value very close to 1. We set  $a_{\langle i,j \rangle} = 1$  for simplicity.
- <sup>16</sup> T. Valla, A. V. Federov, Jinho Lee, J. C. Davis and G. D. Gu, Science, **314**, 1914 (2006).
- <sup>17</sup> Agterberg and Tsunetsugu, Nature Physics **4**, 639 (2008).
- <sup>18</sup> C. P. Chou, N. Fukushima, and T. K. Lee, arXiv:0807.1875 (unpublished).

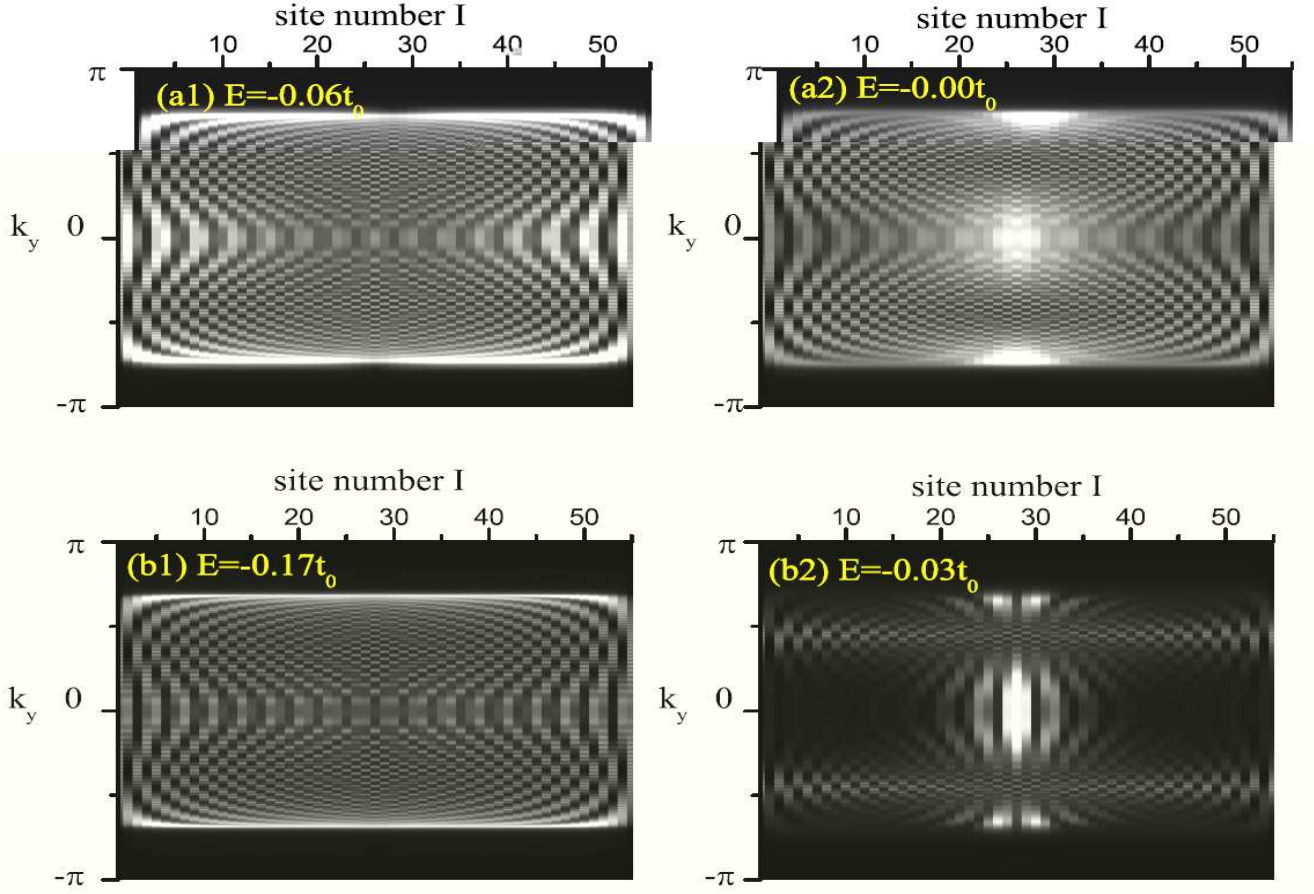


FIG. 2: (Color online) The spatial ( $I$ ) and wavevector ( $k_y$ ) dependence of the quasiparticle spectral weight  $A_{I,k_y}(E)$  for the simplified model ( $H_s$  in Eq[10]) with an isolated site-centered anti-phase domain wall in a d-wave SC. The parameters are the same as that used in Fig[1]. Panels (a) and (b) are for  $\tilde{\Delta}_p = 0.02$  (0.08), respectively. The energies  $E$  corresponds to the Andreev bound states (ABS) in the r.h.s. panels and the bulk SC gap in the l.h.s. panels as shown in Fig[1a,b]. In panel (a2) ABS extends away from the domain wall at site 28 into the bulk of the superconducting state due to  $|\Delta|/E_F \ll 1$ , while in panel(b2) where  $|\Delta|$  is much larger the ABS is much more confined in a small region around the domain wall. For the states close to the SC gap, small  $\Delta$  leads to a more homogeneous state, while moderate  $\Delta$  results in a great suppression of the state close to domain wall.

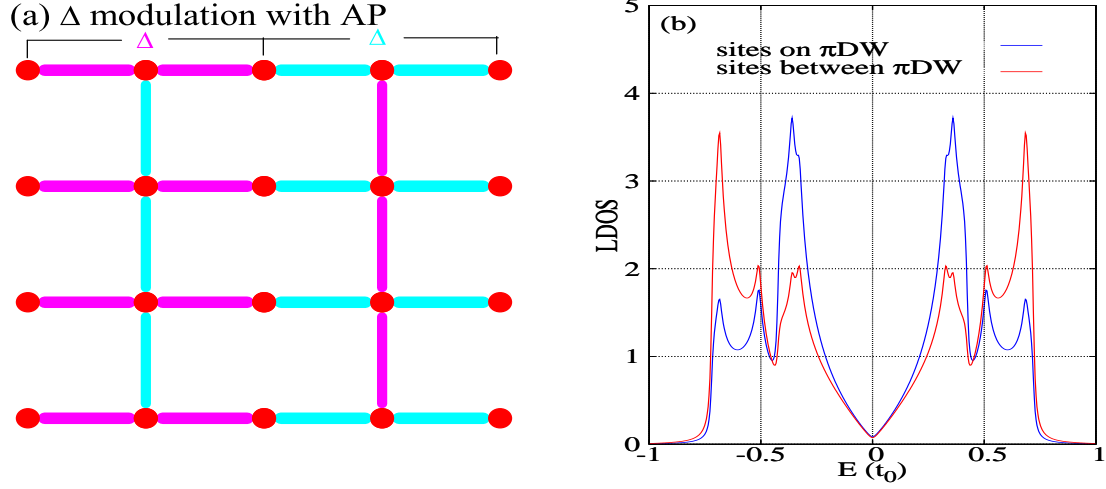


FIG. 3: (Color online) (a) Schematic illustration of the modulation of the pairing parameter  $\Delta$  for the simplified model (Hamiltonian  $H_s$  defined in Eq[10]) for dSC state with periodic site-centered anti-phase domain walls with the shortest periodicity of  $L_x = 4$ . The anti-phase pattern of  $\Delta$  is illustrated by the color scheme. (b) Local density of states (LDOS) with parameter values as doping concentration  $\delta = 0$  and  $\tilde{\chi}_p = \tilde{\Delta}_p = 0.2$ . The domain walls are close to each other, they form bands with weak dispersion along  $k_x$  but strong dispersion along  $k_y$  parallel to the domain wall. At half filling, these bands display an anisotropic nodal structure as demonstrated in Eq[13] and by the low energy LDOS behavior.

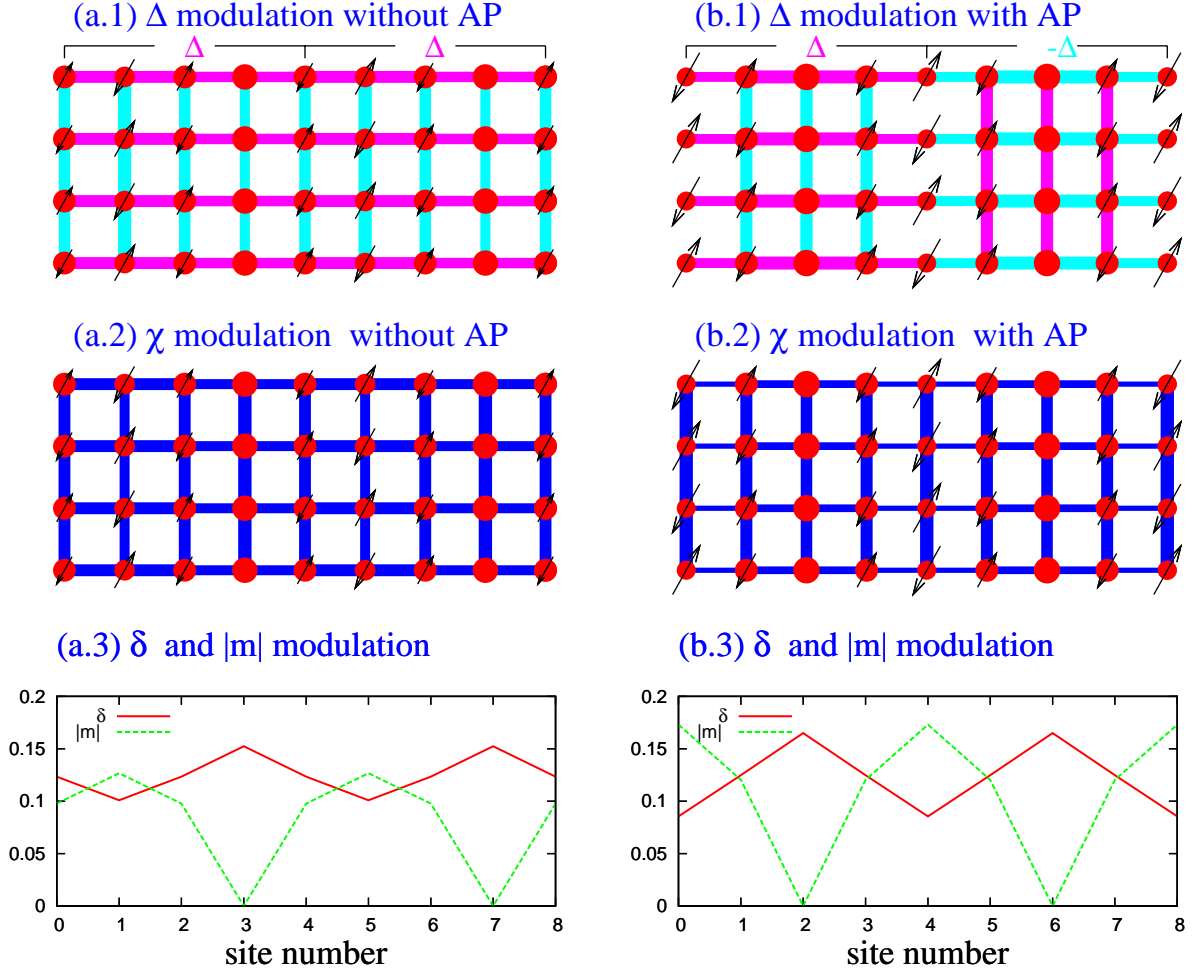


FIG. 4: (Color online) Schematic illustration of the modulations of the parameters pairing amplitude  $\Delta$ , hopping amplitude  $\chi$ , hole concentration  $\delta$  and antiferromagnetic moment  $m$ , for two states: SDW+CDW+dSC<sup>s</sup> [panels (a)] and SDW+CDW+APdSC<sup>s</sup> [panels (b)] (without and with site-centered anti-phase domain walls). The average doping is  $1/8$  and the periodicity  $L_x = 8$ . In panels (a/b 1-2) The amplitudes  $\Delta$  and  $\chi$  are denoted by the width of the bond, the spatial modulation of the staggered antiferromagnetic moment  $m_i$  is denoted by the arrows, the hole concentration modulation is represented by the size of the dots. The anti-phasing of  $\Delta$  in panel(b.1) is illustrated by the different color pattern at either side of the domain wall with cyan (magenta) for positive (negative) value. D-wave pairing symmetry is still preserved between two neighboring domain walls. The anti-phase domain walls coincide with the sites which have the largest sublattice antiferromagnetic moment and smallest hole concentration. However, for the case without SDW, the domain walls locate at the sites with the largest hole concentration.<sup>8</sup> Panels (a/b 3) show the spatial hole density (red solid) and the AF moment (green dash) modulations. The site-centered anti-phase domain walls lead to an anisotropy of  $\chi$ , and an enhancement of the hole density and antiferromagnetic moment modulation.

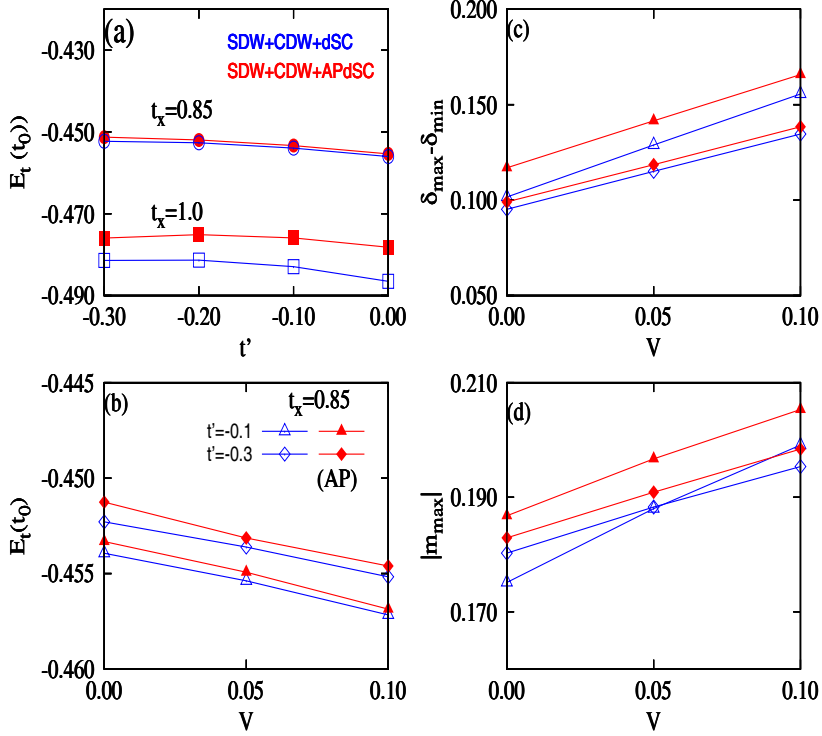


FIG. 5: (Color online) (a) The energy (shown in Eq[5]) dependence of the two states SDW+CDW+dSC<sup>s</sup> and SDW+CDW+APdSC<sup>s</sup> (without and with site-centered anti-phase domain walls) on the nnn hopping integral  $t'$  for isotropic and anisotropic nn hopping ratio  $t_x/t_y$ . The energy unit is  $t_0 = 300meV$ . The nnn hopping integral  $t'$  does not but anisotropic  $t_{x(y)}$  and  $J_{x(y)}$  do help to push the energy of SDW+CDW+APdSC<sup>s</sup> state (the solid and red symbol) closer to SDW+CDW+dSC<sup>s</sup> state (the open and blue symbol). Square (circle) symbols are for the values  $t_x/t_y = 1.00(0.85)$ . Panels (b, c, d): the energy, charge and magnetization moment modulations of these two states with additional external potentials which are imposed to enhance the charge and magnetic modulations by shifting the local potential by  $+V$  ( $V > 0$ ) up for the sites with the largest antiferromagnetic moment and  $-V$  down for the sites with zero antiferromagnetic moment. A substantial anisotropy  $t_x/t_y = 0.85$  is used. The diamond (triangle) symbols are for  $t' = -0.3(-0.1)$ . The larger antiferromagnetic moment and hole concentration modulations drive the energy difference smaller between the two states.

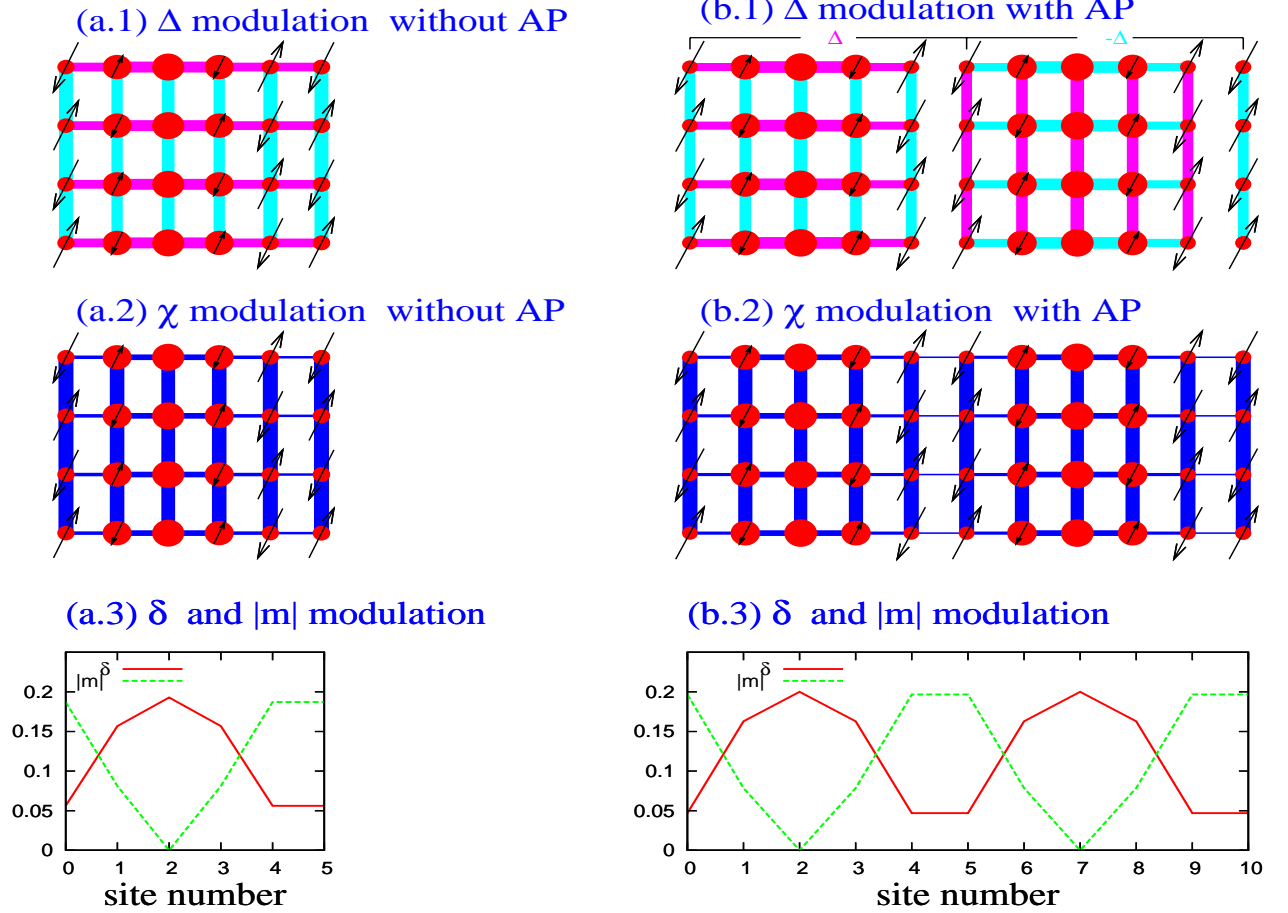


FIG. 6: (Color online) Schematic illustration of the modulations of the parameters pairing amplitude  $\Delta$ , hopping amplitude  $\chi$ , hole concentration  $\delta$  and antiferromagnetic moment  $m$ , for two states: SDW+CDW+dSC<sup>b</sup> [panels (a)] and SDW+CDW+APdSC<sup>b</sup> [panels (b)] (without or with bond-centered anti-phase domain walls). The average doping is  $1/8$  and the periodicity  $L_x = 10$ . As shown in panel (b1) the anti-phase modulation of the pairing  $\Delta$  is bond-centered with the domain wall located at the bonds connecting two nn sites with maximum stagger antiferromagnetic moment  $\pm|m|$  along x direction. The energy difference between the two states with and without bond-centered domain wall is even smaller than the case for site-centered domain wall with anisotropic nn hopping  $t_x/t_y = 0.85$ . The modulation magnitude of the hole density and antiferromagnetic moment in these two states are close to each other.

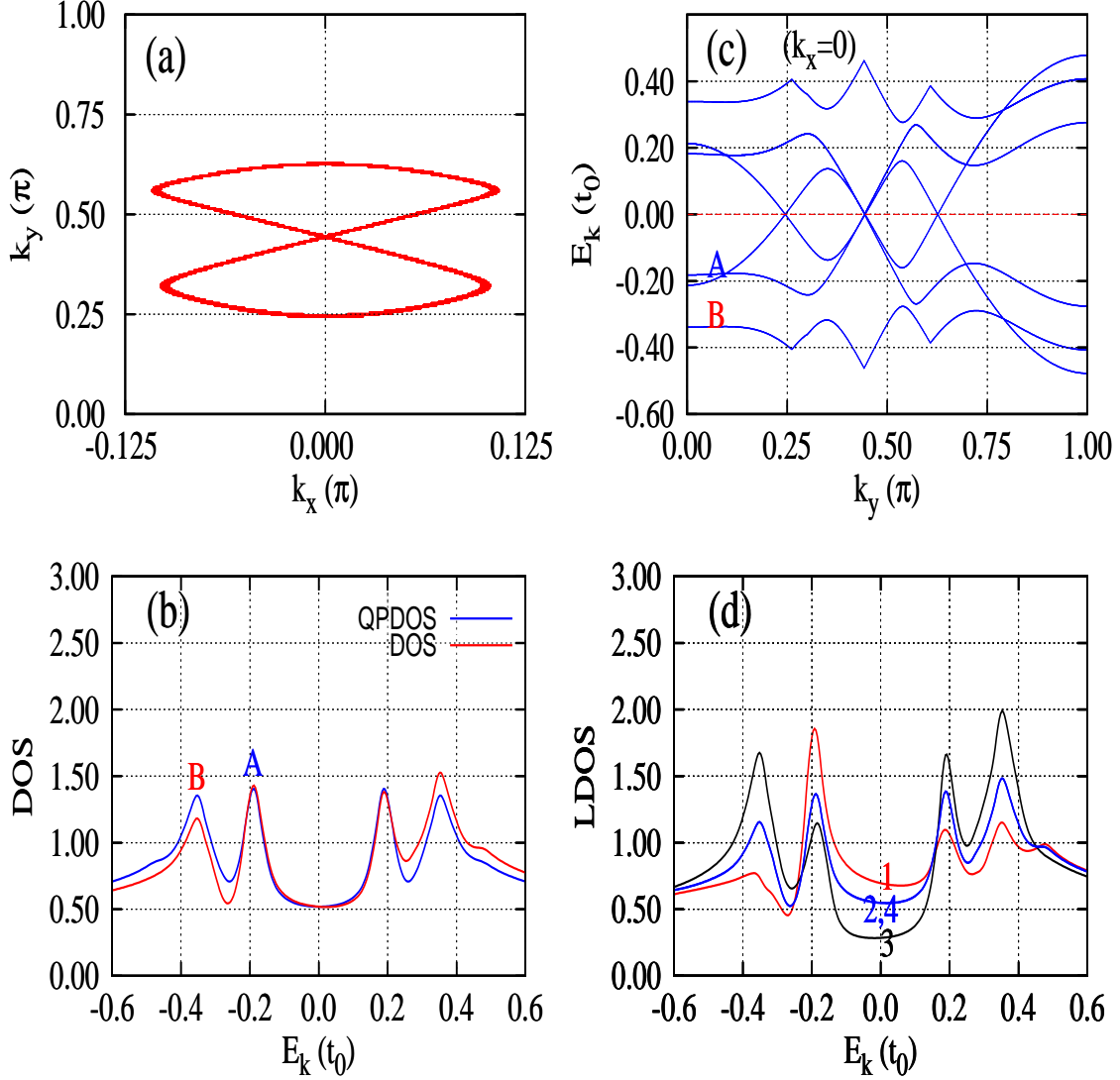


FIG. 7: (Color online) dSC state with site-centered anti-phase domain wall but without antiferromagnetism (doping concentration  $\delta = 1/8$ ,  $t' = 0.0$ ,  $V = 0$ , and a supercell  $L_x = 8$ , the energy unit is  $t_0 = 300meV$ ). The pattern for the pairing amplitude  $\Delta$  is similar to the case shown in Fig[4]. (a) Fermi surface in the reduced Brillouin zone. (b) Quasiparticle (QP) DOS (blue) and average DOS (red). The two peaks A and B at negative energies are a consequence of the flat dispersion along  $k_y$  direction [shown in panel (c)] formed by the propagating of Andreev bound state along  $y$  direction. (d) Local DOS (LDOS), near to the Fermi level the largest portion of the density of states is at the center of the domain wall.



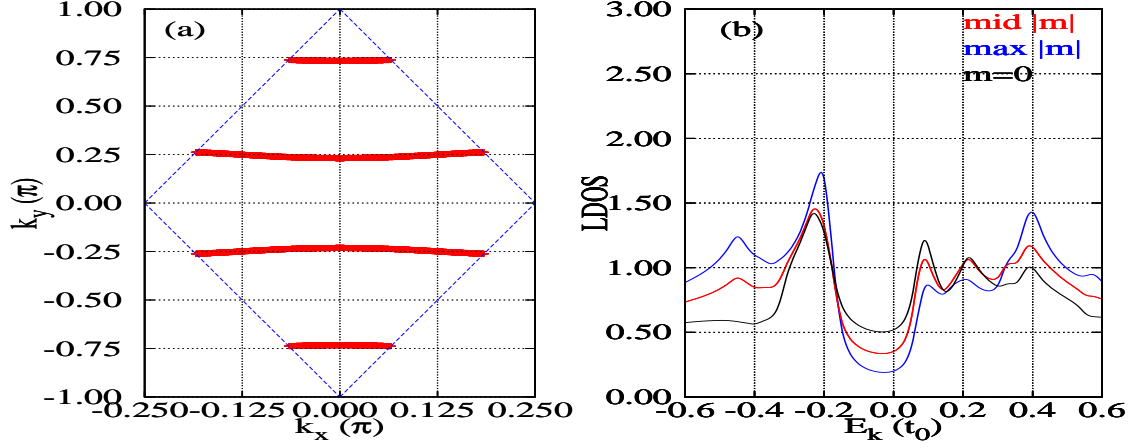


FIG. 8: (Color online) SDW state (without dSC  $\Delta = 0$ ) with a periodicity of  $L_x = 8$  and an average doping concentration  $\delta = 1/8, t' = -0.10$  (the energy is in unit of  $t_0 = 300\text{meV}$ ). The antiferromagnetic sublattice moment pattern is the same as that shown in Fig[4]. (a) Fermi surface in reduced Brillouin Zone. (b) Local density of states (LDOS). Note that this SDW state is a metallic state.

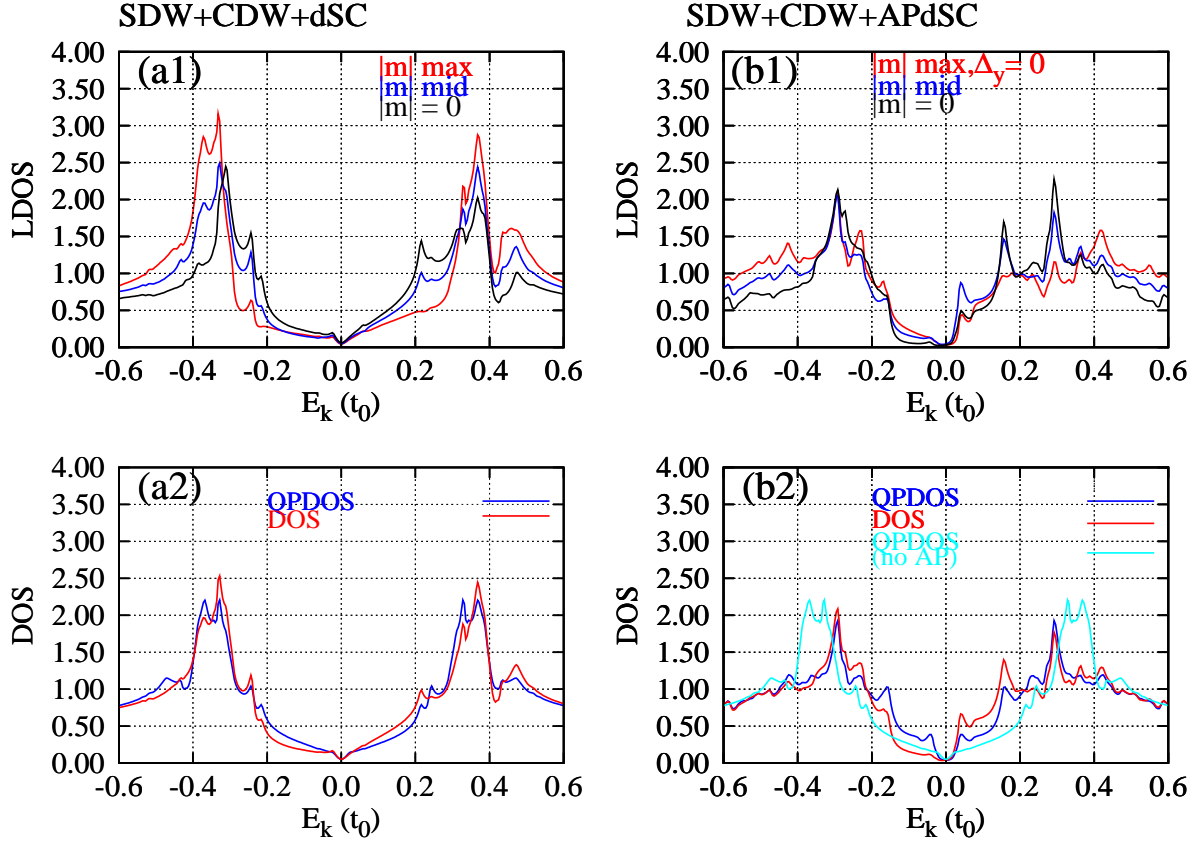


FIG. 9: (Color online) SDW+CDW+dSC<sup>s</sup> and SDW+CDW+APdSC<sup>s</sup> states (without or with site-centered anti-phase domain wall). The upper figures (a1, b1) show the local density of states (LDOS) at the three inequivalent sites with max  $|m|$ , zero  $|m|$ , and the middle site. (doping  $\delta = 1/8$ ,  $t' = -0.1$ ,  $V = 0$ , and isotropic  $t_x = t_y$ ). The energy is in unit of  $t_0 = 300meV$ . The lower figures (a2, b2) show the average DOS and quasiparticle (QP) DOS. In order to facilitate the comparison between the states with and without the domain wall in panel (b2) the cyan curve is the QP DOS for the SDW+CDW+dSC<sup>s</sup> state, replotted from panel (a2). A small gap opens at zero energy. However, a substantial part of the DOS located at lower energy is pushed to closer to the Fermi level. This may be the reason that the opening of a gap in the SCW+CDW+APdSC<sup>s</sup> state does not lead to a lower energy relative to the state without the domain wall. Note that a small broadening  $\delta = 0.004t_y$  is used to smooth the curve. The nodal behavior in SDW+CDW+dSC<sup>s</sup> state is not a general phenomenon. For larger  $t'$ , anisotropic  $t_{x(y)}$ , or external additional potential this nodal structure may disappear. Also for other cases, (e.g.  $t' = 0, t_x = 1, V = 0$ ) no gap opens in SDW+CDW+APdSC<sup>s</sup> state.